Enhanced Elastic-Foundation Analysis of Balanced Single Lap Adhesive Joints

A Thesis Presented

by

Hamed Abdi

to

Department of Mechanical and Industrial Engineering

in partial fulfillment of the requirements

for the degree of

Master of Science

in the field of

Mechanical Engineering

Northeastern University

Boston, Massachusetts

December 2017

TABLE OF CONTENTS

1. INTRODUCTION ……. 1

2. ADHESIVE FAILURE STRESS FROM ELASTIC FOUNDATION ANALYSIS ……..……...…. 5

3. THE ACCURACY OF PEAK PEEL STRESS FROM BEAM-ON-ELASTIC-FOUNDATION (BEF) SOLUTIONS …….……..…....……... 13

4. SIMPLIFIED EXPRESSIONS FOR JOINT-EDGE MOMENT WITH ROTATION …….……. 22

   4.1) Beam-Column Result for Simply Supported Adherends ……... 25

   4.2) Beam-Column Result for Fixed-Slope Ends …….. 30

5. CONCLUSIONS …….……. 33

6. APPENDIX …….. 36

   6.1) Appendix 1: an equivalent stress for pressure-sensitive yield ……... 37

   6.2) Appendix 2: Derivation of beam-column results ……...… 38

7. REFERENCES …….…… 41

LIST OF FIGURES

Fig.1 Canonical loading of a SLJ: symmetric with no force obliquity, hence resulting in maximum edge moment …….. 6

Fig.2 (A) Peak peel stress versus bond length (B) Peak shear stress versus bond length. Each stress is normalized by its long-joint value, and each length is normalized by the characteristic length for that stress. For joints susceptible of elastic foundation analysis, $\lambda_s \gtrsim \lambda_p$ so the shear stress falls no faster than the peel stress climbs, as a function of D .. 8

Fig. 3 Peak (joint-end) failure stresses from BEF solution, versus bond length normalized by shear characteristic length, for one possible SLJ ($E = 70\text{GPa}$, $t = 10\text{ mm}$, $\nu = 0.33$, $E_a = 1\text{ GPa}$, $t_a = 0.2\text{ mm}$, $\nu_a = 0.4$, $F = 158.5\text{ N/m}$). The right ordinate reflects normalization by adherend mean tensile stress F/t ……... 11

Fig.4 Original centerline loading, replacement by forces and centroidal moments $M = Ft/2$, decomposition into symmetric (sym responsible for peel stress only) and antisymmetric (asym responsible for shear stress only), and further decomposition of sym into opposed-moments loading and axial loading ……. 16

Fig.5 A) Comparison between FEA and BEF peel stress distribution for a long metal-epoxy joint. B) Poisson-driven joint end FEA peel stress drop, FEA peel stress peak distance from the joint end, $|x'_P|$, BEF joint-end peel stress slope, original and corrected BEF peak stresses are shown ……. 18

Fig. 6 A) Position $|x'_P|$ of the peel stress peak (relative to the joint end) as determined by FEA. B) The results are reasonably fitted by a polynomial in ν_a …….. 19

Fig. 7. Region of applicability of modified Elastic Foundation formula for long-joint peak peel stress: For each upward sloping line (dependent on adhesive Poisson Ratio), accurate

predictions are expected in the direction of the arrow. For comparison, the Goland & Reissner proposed region of validity for elastic foundation analysis is shown by an arrow on the downward sloping blue line. The right half of the plot involves increasingly thick adhesive 20

Fig. 8 A) general loading case consistent with 180^o rotational symmetry must reduce to B) a force transmitted through O 24

Fig. 9 A) Timoshenko beam-column under tension B) schematics of half-specimen with pinned ends, where adhesive midpoint O is fixed in space by symmetry arguments, and adherend end B translates horizontally with zero moment. a is half the centroid separation of the two adherends, and $D/2$ is half the overlap length C) schematics of half-specimen with fixed-slope ends, where adhesive midpoint O is fixed in space by symmetry arguments, and adherend end B translates horizontally with zero slope 26

Fig. 10 A) Plot for determining edge moment of pinned-end assemblies, as a function of tensile load T. Curves are a function of L/D, approaching the straight asymptote as L/D approaches infinity. Near zero load, the moment arm is determined by the undeformed force line of action between the loading pins. B) Similar plot for determining edge moment of fixed end-slope assemblies, as a function of tensile load T. Curves are a function of L/D, where the uppermost curve has $L/D = 2$, the lowermost has $L/D = 10$, and the orange curve is for $L/D \to \infty$. At low load, the effect of a fixed-slope end on reducing moment can be deduced by a linear beam calculation 29

ABSTRACT

Conventional single-lap adhesive joints between identical adherends achieve ultimate strength only after significant inelastic deformation of the adhesive and perhaps also the adherends. However purely elastic analysis provides insights and is relevant to fatigue initiation or brittle failure. We extend classical beam on elastic foundation results, both 'within the bond' (deriving more-accurate peak peel stress from the joint-edge moment) and 'beyond the bond' (determining the edge moment from adherend dimensions, remote boundary conditions, and load).

Within the bond, we show that peak adhesive equivalent stress and principal stress are minimized when the bond length exceeds four characteristic lengths of the elastic-foundation shear stress equation. This makes simplified 'long' joint formulas useful for initial design. We then examine how well the long-joint predicted peak peel stress matches plane strain finite element analysis, and empirically capture a peel-stress end effect due to nonzero adhesive Poisson ratio. With this end-effect correction, the limit of useful accuracy can be expressed as a ratio of (adherend axial stiffness) to (adhesive axial stiffness) being > a number of order 10^2-10^3 depending on Poisson ratio. This limit supplements the Goland and Reissner proposed applicability limit for elastic foundation analysis, expressed as a limiting ratio of through-thickness or vertical stiffnesses.

Outside the bond, Timoshenko-style beam-column expressions are used to derive a simplified joint-edge moment factor. While similar in spirit to the edge-moment determination of Goland and Reissner for infinite-length pinned adherends, treating the bond region as a rigid block leads to simpler nonlinear expressions, and captures the moment-reducing benefits of shorter (finite-length) adherends and fixed-slope end

conditions. Joint rotation effects become dominant when tensile load times adherend free length square is larger than the adherend bending stiffness. Then joint rotation magnitude depends on the ratio of the tensile load times lap length square to adherend bending stiffness.

Chapter 1

INTRODUCTION

1. Introduction

The single lap joint (SLJ) is common because fabrication is so convenient. The need for adherend dimensional precision is low, and virtually no forming or machining is required. The already-flat surfaces of the bars or sheets to be joined are simply overlapped with adhesive, squeezed together, and fixtured at a desired separation until the adhesive hardens. While early analyses of lap joint adhesive stress were strictly elastic in character, it is now recognized that the ultimate strength of aerospace sheet metal bonds is developed only after plastic straining of the adhesive and possibly adherends. Even so, simple elastic analyses are not irrelevant as they provide a foundation for understanding joint mechanics. In addition, there may be joints for which brittle fracture or fatigue initiation are a greater concern than ultimate strength involving plasticity. It is from that perspective that this purely elastic investigation was conducted.

Goland and Reissner introduced the partition of lap joint analysis into ‘inner’ and ‘outer’ problems. For the inner problem they assumed the application of joint-edge force and bending moment. Then for the case of significant through-thickness adhesive compliance, they developed the well-known approximate beam-on-elastic-foundation model, and computed peak peel stress due to those edge loads. For the outer problem, they used the governing equation for a beam with tension (the adherend), connected to a finite-length double-thickness beam (the joint region). Their main resulting formula gave the edge moment applied to the joint region, as a function of load, for the case of infinite length adherends with moment-free end supports. Of course, the foregoing is far from a complete list of the accomplishments in their seminal paper.

Although credible numerical elastic-plastic nonlinear analyses are now routine, specific quantitative results are not an ideal design tool. One also needs insight into trends and limits, and if possible, simple algebraic estimates to guide a design approach. The purpose of this investigation is to extend certain aspects of elastic lap-joint analysis, with the desired outcome of useful simple formulas.

In chapter 2, we justify a focus on 'long' joints which exhibit length-independent peak stresses. We start with well-known elastic-foundation formulas for averaged peel and shear stress in the adhesive of finite-length joints (such through-thickness smeared values are quite representative of adhesive midline stresses, as long as the joint is well modeled as beams connected by an elastic foundation – according to Goland and Reissner, that is when the elastic layer vertical compliance is not too small). Assuming approximately zero midline axial strain, plane-strain elastic relations are used to approximate all adhesive stress components from the peel and shear stress, permitting the equivalent stress and greatest principal stress to be computed. Since their peak values are always found at the joint ends (apart from a numerically determined end-effect stress reduction covered in chapter 3), we examine those joint-end values as a function of overlap length. It is observed that the peak 'equivalent stress' (for pressure-independent and pressure-sensitive yield) and peak principal stress reduce towards asymptotically minimum values as the joint is lengthened beyond about four characteristic lengths of the shear stress equation. For design purposes, it therefore seems reasonable to specify that joints should routinely exceed this minimum length. This permits use of the substantially simpler long-joint peak-stress formulas presented by Bigwood and Crocombe.

For such 'long' joints, chapter 3 compares the peel stress σ determined by elastic foundation analysis to σ_{yy} on the adhesive midline computed by plane strain finite element analysis. For zero Poisson ratio of the adhesive, these match quite well all along the midline, over a large range of joint parameters. But for nonzero adhesive Poisson ratio an end effect is observed (over an axial distance proportional to the geometric mean of adhesive thickness and adherend thickness) that truncates the peel stress peak due to loss of horizontal constraint. By curve fitting we provide an empirical expression for the end-effect distance, and combine this with the beam on elastic foundation (BEF) stress solution to approximate the finite element analysis (FEA) peel stress peak (which is always lower than the unmodified BEF peak).

When the corrected elastic foundation peak peel stress is compared to the peak peel stress computed by FEA, agreement is good within a 'region of applicability' in joint-parameter space, whose boundary is based on R_a, the ratio of adherend to adhesive axial stiffness's. This supplements the well-known Goland and Reissner applicability boundary for elastic foundation analysis, which may be expressed in terms of the ratio R_v of through-thickness (vertical) stiffnesses. Both criteria agree in excluding too-stiff adhesive from elastic-foundation analysis.

In chapter 4 we turn to the 'outer' problem, in order to extend the Goland and Reissner analysis of edge moment factor, k. We adapt the well-known beam-column formalism presented in Timoshenko and Gere, and approximate the thick overlap region as a rigid block. This allows us to give results for adherends of finite length, and include not only moment-free but fixed-slope end conditions. The resulting edge-moment expressions are both more general and simpler.

There exists an extensive literature on the simplified elastic analysis of single lap joints, as outlined in da Silva et al and extended to dynamic loading by Vaziri et al and others. Many investigators including Goland and Reissner, Volkersen and Hart-Smith used the elastic-foundation approach to investigate approximate through-thickness shear and peel stress distributions of a relatively flexible adhesive layer. In addition, geometrical nonlinearity, which arises from tension rotating the joint region to bring remote adherends closer to coaxial alignment, was long ago recognized by Goland and Reissner. They used axially-loaded beam analysis to determine the edge moment (i.e., the adherend centroidal bending moment at the joint edge) for infinitely long, pinned adherends. Luo and Tong reviewed this and other treatments of rotation.

In addition to many analytical investigations, finite element analyses in 2D and 3D have been performed by Adams and Peppiatt, Her, Li and Lee-Sullivan, Tsai and Morton, Goncalves et al, Ashrafi et al, Haghpanah et al among others. Some of these were elastic-only, while others included adhesive and/or adherend plasticity. To navigate this large literature, we have relied on authoritative and comprehensive reviews by Minford, Da Silva et al, and Adams et al In the publications we have explored, we have not encountered the results developed here.

Chapter 2

ADHESIVE FAILURE STRESS FROM ELASTIC FOUNDATION ANALYSIS

2. Adhesive Failure Stress from Elastic Foundation Analysis

The purpose of this chapter is to show that 'long' joints (defined relative to the characteristic length λ_s of the elastic-foundation equation for adhesive shear stress) exhibit the lowest peak 'equivalent stress' responsible for yield, and also the lowest peak principal stress (responsible for brittle fracture). Assuming that designers will generally exploit this strength advantage, it seems reasonable to initiate designs with the simple 'long joint' formulas for peak stress, as provided by Bigwood and Crocombe.

Consider a joint with 180^o symmetry loaded by a force in the joint plane (thus giving rise to maximum adherend bending moment with no shear force, see Fig. 1). The well-known elastic-foundation governing equation for peel stress σ is:

$$\frac{d^4\sigma}{dx^4} + \frac{4\sigma}{\lambda_p^4} = 0 \tag{1}$$

where the peel characteristic length λ_p is defined by $\lambda_p = \sqrt[4]{\frac{\bar{E}t^3 t_a}{6\bar{E}_a}}$.

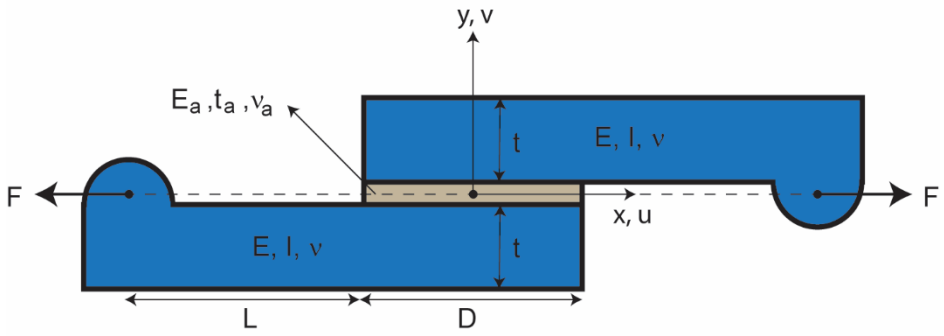

Fig.1 Canonical loading of a SLJ: symmetric with no force obliquity, hence resulting in maximum edge moment.

Here we have used equivalent Young's moduli with an overbar, defined as follows: For the adherend it is the plane-strain Young's modulus $\bar{E} = E/(1-\nu^2)$, although this won't properly represent axial stretching unless $w >> \max(L, D)$, where L is the free adherend length, D is the

joint overlap and w is the specimen width perpendicular to the axis of loading. For adhesive away from the edges and corners of the joint, we use the horizontally constrained modulus:

$$\overline{E}_a = \frac{E_a(1-\nu_a)}{(1+\nu_a)(1-2\nu_a)} \tag{2}$$

(While this expression suggests unbounded stiffness as $\nu_a \rightarrow 0.5$, in fact E_a should not be taken as independent of ν_a. Polymer bulk modulus K_a arising from interatomic repulsive forces is relatively unvarying in the range of $1-5$ GPa, whereas the moduli capturing distortional behavior such as $E_a = 3K_a(1-2\nu_a)$ and $G_a = (3K_a/2)(1-2\nu_a)/(1+\nu_a)$ both reduce toward zero as Poisson ratio approaches 0.5. It can be useful to recast some of the below expressions with the adhesive moduli expressed in terms of K_a.)

The solution of the peel stress equation for an arbitrary length bond subjected to an applied joint-edge moment per unit width $Ft/2$ (where F is force per unit width of specimen) is a well-known symmetric expression:

$$\sigma = \frac{Ft}{\lambda_p^2}\left[A\sinh\left(\frac{x}{\lambda_p}\right)\sin\left(\frac{x}{\lambda_p}\right) + B\cosh\left(\frac{x}{\lambda_p}\right)\cos\left(\frac{x}{\lambda_p}\right)\right] \tag{3}$$

where

$$A = \frac{\left[\sinh\left(D/(2\lambda_p)\right)\cos(D/(2\lambda_p)) + \cosh\left(D/(2\lambda_p)\right)\sin\left(D/(2\lambda_p)\right)\right]}{\sinh\left(D/\lambda_p\right) + \sin\left(D/\lambda_p\right)} \tag{4}$$

$$B = \frac{\left[\sinh\left(D/(2\lambda_p)\right)\cos(D/(2\lambda_p)) - \cosh\left(D/(2\lambda_p)\right)\sin\left(D/(2\lambda_p)\right)\right]}{\sinh\left(D/\lambda_p\right) + \sin\left(D/\lambda_p\right)} \tag{5}$$

The peak value of the peel stress occurs at the adhesive ends where $x = \pm D/2$, with magnitude found through algebraic manipulations and use of identities:

$$\sigma_P = \frac{Ft}{2\lambda_P^2}\,\frac{\sinh\left(D/\lambda_p\right) - \sin\left(D/\lambda_p\right)}{\sinh\left(D/\lambda_p\right) + \sin\left(D/\lambda_p\right)} \tag{6}$$

Peak peel stress normalized by its long-joint value, $\overline{\sigma}_P = \sigma_P(2\lambda_P^2)/(Ft)$, is plotted versus D/λ_p in Fig. 2A, to show the effect of bond length.

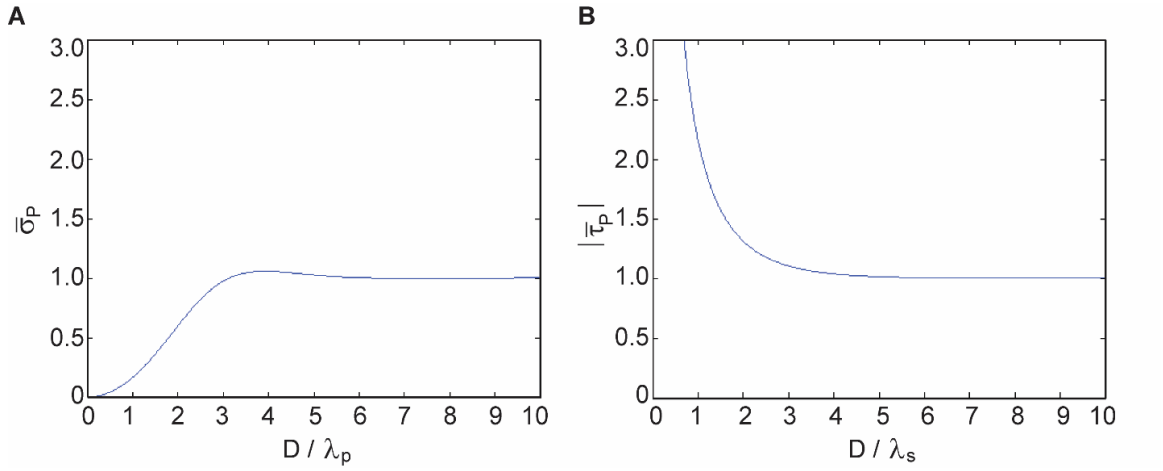

Fig.2 (A) Peak peel stress versus bond length (B) Peak shear stress versus bond length. Each stress is normalized by its long-joint value, and each length is normalized by the characteristic length for that stress. For joints susceptible of elastic foundation analysis, $\lambda_s \gtrsim \lambda_p$ so the shear stress falls no faster than the peel stress climbs, as a function of D.

A similar brief development is followed for adhesive shear stress. The elastic-foundation governing equation for shear stress is:

$$\frac{d^3\tau}{dx^3} - \frac{8G_a}{\bar{E}tt_a}\frac{d\tau}{dx} = 0 \tag{7}$$

The shear stress characteristic length is $\lambda_s = \sqrt{\frac{\bar{E}tt_a}{8G_a}} = \sqrt{\frac{\bar{E}tt_a(1-\nu_a)}{4\bar{E}_a(1-2\nu_a)}}$. The symmetric solution for an arbitrary bond length is:

$$\tau(x) = -\frac{F}{2\lambda_s}\left[\frac{\cosh(x/\lambda_s)}{\sinh(D/2\lambda_s)}\right] \tag{8}$$

The peaks of this expression occur at the joint ends $x = \pm D/2$. Peak shear stress normalized by its long-joint value $|\bar{\tau}_P| = |\tau_P|(2\lambda_s/F)$ is plotted versus D/λ_s in Fig. 2B.

The peak values of peel and shear stress as functions of bond length show that the peak shear stress starts at infinity (for a short bond, it is of order F/D) and reduces toward a constant value. For $D/\lambda_s > 4$ the difference between τ_p and its infinite-length value becomes less than 5%. In contrast, the peak peel stress starts at zero and climbs toward a constant value (with a modest

6% overshoot). For $D/\lambda_p > 5$ the difference between σ_p and its infinite-length value becomes less than 5%. The designer must therefore consider the tradeoff between shear stress reduction and peel stress increase due to bond length. The rational way to resolve these competing concerns is with a multi-axial failure criterion: determining the peak 'equivalent' stress σ^e if yielding or fatigue initiation is the design issue, or determining the peak greatest principal stress σ_I if brittle fracture is the key concern. Such stress measures require all six stress components at each point.

But before estimating these we show that λ_s is usually greater (and never much less) than λ_p. (In other words, the peak shear stress drops to its asymptotic long-joint value only after the peak peel stress has increased, so we expect no intermediate-length minimum for typical combined-stress measures.) To see this, consider

$$\left(\frac{\lambda_s}{\lambda_p}\right)^4 = \frac{3}{8}\frac{\overline{E}/t}{\overline{E}_a/t_a}\frac{(1-\nu_a)^2}{(1-2\nu_a)^2} = R_V\frac{3}{8}\left(\frac{1-\nu_a}{1-2\nu_a}\right)^2 \qquad (9)$$

where we have introduced R_V, the ratio of vertical through-thickness stiffness of adherend and adhesive, defined by $R_V = \frac{\overline{E}/t}{\overline{E}_a/t_a}$. According to Goland and Reissner, R_V should exceed 10 for an adhesive bond to be describable by a beam-on-elastic-foundation model, which leads to $\lambda_s > \lambda_p$ for any value of ν_a. But even if we discount the Goland and Reissner criterion (an alternative condition for elastic-foundation accuracy is discussed in the next chapter), we may take account of realistic joint parameters. In a typical metal-epoxy joint, t_a would have to shrink below a few microns for λ_s to fall below λ_p. Therefore, for most practical purposes λ_s is the bond characteristic length, and stress can only be minimized by taking the joint 'long' (i.e. $D > 4\lambda_s$).

Although elastic-foundation analysis provides only the peel and shear stresses, we may estimate all stress components on the adhesive centerline as follows: in plane-strain adhesive loading $\varepsilon_{zz} = \varepsilon_{yz} = \varepsilon_{xz} = 0$, and we have the expressions for peel stress $\sigma = \sigma_{yy}$ and shear stress $\tau = \tau_{xy}$. For a final condition, we assume adhesive strains ε_{yy} and ε_{xy} to be considerably greater

than ε_{xx} (which is approximately bounded by the axial strain of stiff adherends), and adopt the approximation $\varepsilon_{xx} = 0$. Then the other two direct stresses are $\sigma_{xx} = \sigma_{zz} = \sigma\nu_a/(1-\nu_a)$.

In metal plasticity, the most common equivalent stress (for predicting either yield or fatigue initiation) is the von Mises stress, equal to $\sigma_{VM} = \sqrt{3J_2}$, where J_2 is the second invariant of the deviatoric stress. For pressure-sensitive adhesive yielding (see Appendix 1) we may modify this to $\sigma^e = \sqrt{3J_2 + (k_c - k_t)I_1}$, where I_1 is the first invariant of the stress, and k_c , k_t are axial yield stresses in compression and tension respectively, both considered positive. An equivalent stress with pressure sensitivity may then be calculated from peel and shear:

$$\sigma^e = \sqrt{\left(\frac{1-2\nu_a}{1-\nu_a}\right)^2 \sigma^2 + 3\tau^2 + (k_c - k_t)\,\sigma\left(\frac{1+\nu_a}{1-\nu_a}\right)} \tag{10}$$

with yield when $\sigma_e = \sqrt{k_c k_t}$. When $k_c = k_t$ then $\sigma^e = \sigma_{VM}$, the von Mises stress with failure when $\sigma_{VM} = k_t$.

The largest principal stress (for calculating brittle fracture) is calculated as:

$$\sigma_I = \frac{\sigma}{2-2\nu_a} + \sqrt{\left(\frac{1-2\nu_a}{2-2\nu_a}\right)^2 \sigma^2 + \tau^2} \tag{11}$$

In Fig. 3 the peak (i.e., joint-end) equivalent stress for $k_c - k_t = 0, 2, 4, 6$ MPa is plotted versus bond length for a specific joint. Since the joint-end mean stress is highly tensile, the pressure-sensitive equivalent stress is significantly raised, so a given value of σ^e is reached at a lower load or longer joint. (Considering the mean of tensile and compressive strengths $(k_c + k_t)/2$ as a fixed quantity considerably greater than $(k_c - k_t)/2$, the numerical value of $\sigma^e = \sqrt{k_c k_t}$ that defines failure will hardly be affected by $k_c - k_t$.) The first principal stress is also plotted. With just a slight short-joint deviation for the principal stress, all plotted peak stresses reduce monotonically to their minimum values (which reduce with greater characteristic length) after shear stress has fallen, i.e. $D/\lambda_s > 4$. Therefore, maximizing the shear characteristic length and setting $D = 4\lambda_s$ is one possible strategy for efficiently minimizing adhesive equivalent stress.

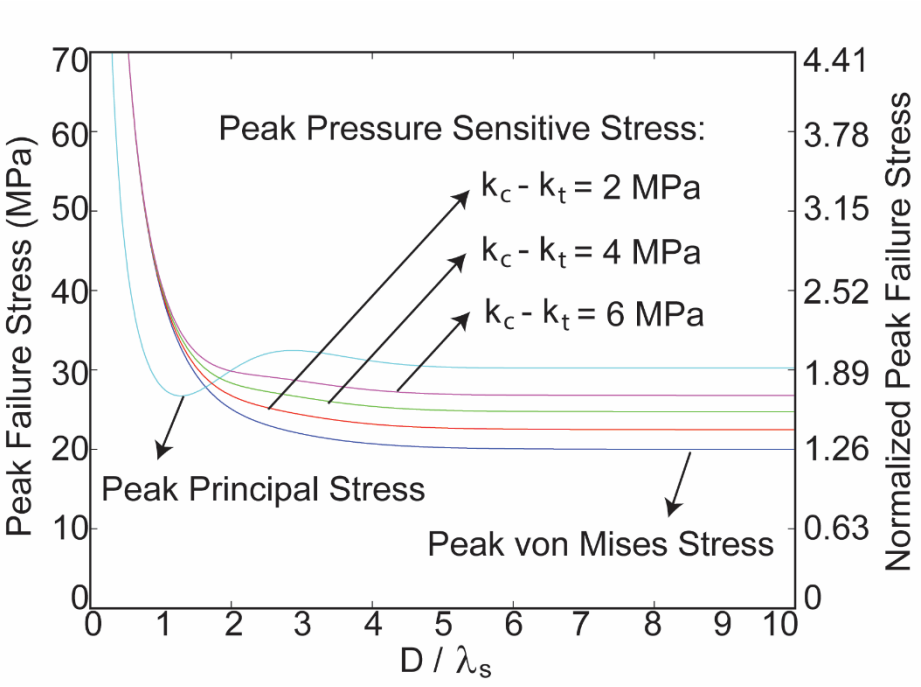

Fig. 3 Peak (joint-end) failure stresses from BEF solution, versus bond length normalized by shear characteristic length, for one possible SLJ ($E = 70GPa$, $t = 10\ mm$, $\nu = 0.33$, $E_a = 1\ GPa$, $t_a = 0.2\ mm$, $\nu_a = 0.4$, $F = 158.5\ N/m$). The right ordinate reflects normalization by adherend mean tensile stress F/t.

Since the plotted equivalent and Principal stress results are strictly proportional to load, they can usefully be normalized (e.g., by the adherend mean tensile stress – see the right hand ordinate) to give load-independent results. But the pressure-dependent equivalent stress does not have this property.

The assumption of a long joint is common in the literature, and the foregoing development shows that realizing it should result in a stronger joint (by elastic analysis). The long-overlap peak (end-of-joint) values derived from Eqs. (6) and (8) are of course especially simple, and conform to the simplified expressions of Bigwood and Crocombe:

$$\sigma_p = \frac{Ft}{2\lambda_P^2} = F\sqrt{\frac{3\bar{E}_a}{2\bar{E}tt_a}} \tag{12}$$

$$\left|\tau_p\right| = \frac{F}{2\lambda_s} = F\sqrt{\frac{2G_a}{\bar{E}tt_a}} \tag{13}$$

We will see in chapter 3 that these long-joint peak values are not quite attained due to end-effect truncation, but we take them as a guide to the magnitudes involved.

It appears to be unsettled why the theoretical inverse dependence of stress on adhesive thickness does not lead to stronger joints when thicker adhesive is tried. (When the analyses are revised to incorporate finite adhesive thickness throughout, the optimum adhesive thickness appears to be of order 70% of adherend thickness.) One reason may be the yielding of adhesive and adherends at peak load, which invalidates the elastic assumptions. But it also appears that experimental investigators did not increase D when greater t_a led to a greater λ_s, thus unintentionally violating the long-joint requirement $D > 4\lambda_s$ and increasing the peak stress. A preferred evaluation of adhesive 'thickness effect' might be to increase all axial and thickness dimensions (including t_a) in proportion, and evaluate whether or not the load at initial yield follows that increase.

It is interesting to compare the peak long-joint values of peel and shear stress. We have:

$$\frac{\sigma_P}{\tau_P} = \frac{t\lambda_s}{\lambda_p^2} = \sqrt{\frac{3(1-\nu_a)}{2(1-2\nu_a)}} \tag{14}$$

which means that the long-joint peak peel stress always exceeds the peak shear stress – a little if $\nu_a = 0$ and a lot if ν_a approaches 0.5. Of course this analysis is premised on a joint-edge moment arm of $t/2$, and the finite rotation to be discussed below (involving strong bonds between long adherends) can potentially reduce the peak peel stress below the peak shear stress.

Using this peel- to shear-stress ratio we may rewrite the failure-stress formulas as either the peak shear or peak peel stress, times a function of Poisson ratio. It seems appropriate to highlight the role of adhesive shear stress, as it dominates each failure criterion when the joint is short, and still plays a major role in the long-joint case.

Chapter 3

THE ACCURACY OF PEAK PEEL STRESS FROM BEAM-ON-ELASTIC-FOUNDATION (BEF) SOLUTIONS

3. The Accuracy of Peak Peel Stress from Beam-on-Elastic-Foundation (BEF) Solutions

In this chapter our purpose is to evaluate the beam-on-elastic-foundation (BEF) long-joint formula for adhesive peel stress, when the joint is loaded by a force in the adhesive midplane, i.e., without the moment-reducing benefits of finite rotation, offset pinned boundary conditions, or fixed-slope boundary conditions. Our approach is to compare the above simple analytical results to the plane-strain finite element analysis (FEA). Qualitative comparison reveals an "end effect" adhesive-stress reduction for nonzero ν_a. We propose an empirical correction for this reduction, then compare the corrected BEF formula to the peak centerline peel stress found by FEA. (Since midline shear stress σ_{xy} must vanish at the free end, τ must also exhibit an end-effect, ignored in this study.)

Consider a joint edge loaded by axial force per unit width F and centroidal bending moment per unit width $Ft/2$. (A more accurate moment expression is $F(t + t_a)/2$, the leading-order correction of a thick-adhesive formulation that distinguishes between beam half-height, and the distance between beam centroid and adhesive centerline. We will use this expression occasionally without adopting the entire thick-adhesive theory.) The long-joint peak peel stress valid for $D > 4\lambda_s$ was given above by:

$$\sigma_P = \frac{1}{2} Ft/\lambda_p^2 \tag{15}$$

where $\lambda_p = \sqrt[4]{\frac{\bar{E}t^3 t_a}{6\bar{E}_a}}$. This stress is proportional to edge moment per unit width but does not explicitly depend on joint length. Maximizing λ_p is clearly beneficial, but only as long as D keeps pace.

For bonds satisfying the long-joint criterion, how well does the BEF solution for adhesive peel stress match the FEA solution? If the adhesive Poisson ratio is small (decoupling the adhesive's vertical stress from its horizontal stress throughout the joint, and thereby eliminating the impact of

axial non-constraint at the adhesive free-end) the BEF and FEA peel stress curves tend to be very similar. However, if adhesive Poisson ratio is not close to zero there will be significant horizontal stresses in much of the joint, while of course the 'constrained modulus' governing vertical strain diverges increasingly from E_a. But at the adhesive free end, the lack of horizontal constraint strongly reduces horizontal and vertical stress, and somewhat reduces vertical stiffness.

One way to understand lap joint adhesive stress analysis is via symmetric / antisymmetric decomposition of the joint-edge loads. (These are represented as beam resultants, but of course the actual stresses will not vary linearly.) As shown in Fig. 4, midplane loading of a joint with 180^o rotational symmetry can be decomposed into joint-edge load cases sym and asym. Sym has reflection symmetry across the adhesive centerline and causes only centerline peel stress. Asym has reflection antisymmetry and causes only centerline shear stress, so it is irrelevant to peel. Sym can further be decomposed into sym-M, symmetric adherend moments, and sym-F, axial forces. Sym-M can be modeled by replacing the lower half of the joint (including half the adhesive layer) with symmetry boundary conditions (vertically fixed, horizontally free). This looks like an end-loaded beam on an elastic foundation. Sym-F is similar to a sandwich panel in tension – the adherend ends experience axial stress, while the adhesive end does not. Away from the ends of a 'long' joint, both materials experience identical axial strain but no peel stress.

Case sym-M is well suited to BEF modeling, except that there is no provision for the altered vertical stiffness and stress at the adhesive end (when Poisson ratio is nonzero). Case sym-F is not simulated by a conventional BEF, but it too will exhibit a Poisson-driven end effect, altering adherend separation and reducing peel stress. Even with zero Poisson ratio, both load cases develop some tension in the adhesive, so the top and bottom adhesive edges experience opposite-sign shear stresses from transferring tension to the adhesive, to an extent and over a region related to adhesive thickness. This will bend the adherends together, adding compressive peel stress. Thus a reduced peel stress is expected at the joint end for multiple reasons, most associated with nonzero Poisson's ratio.

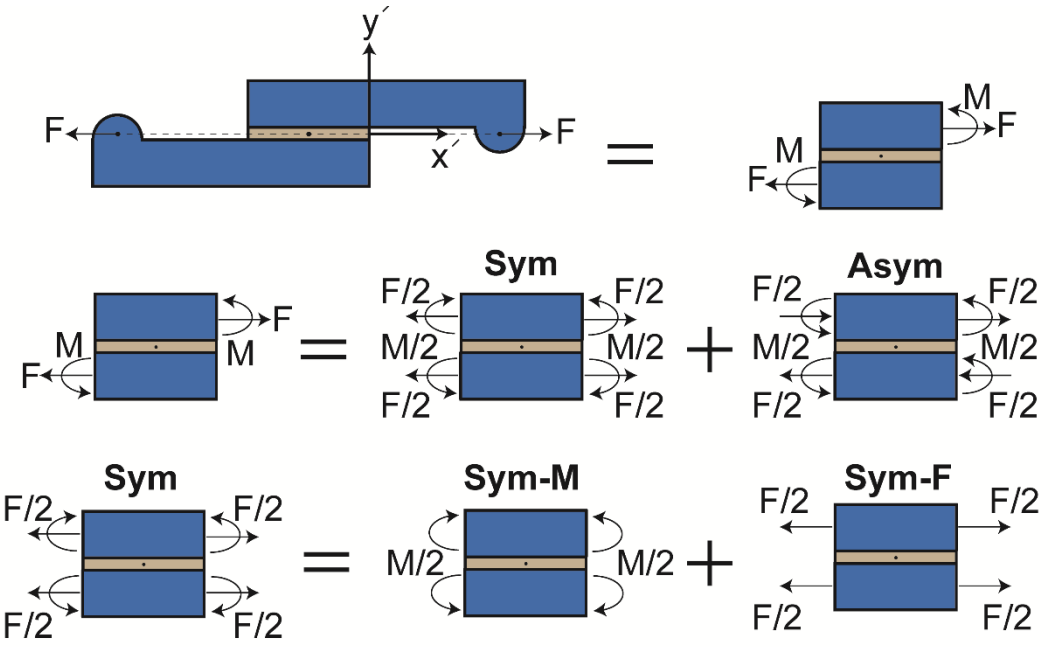

Fig.4 Original centerline loading, replacement by forces and centroidal moments $M = Ft/2$, decomposition into symmetric (*sym* responsible for peel stress only) and antisymmetric (*asym* responsible for shear stress only), and further decomposition of *sym* into opposed-moments loading and axial loading.

ABAQUS linear finite element analysis was used to evaluate 2D linear elasticity deviations from the BEF-calculated peak. The plane strain element CPE4R was selected, with a size of $t/20$ throughout each adherend, and $t_a/20$ throughout the adhesive. (Of course as mentioned above, plane strain assumptions are not entirely right, as the real system is rarely laterally constrained.) Stresses σ_{yy} , σ_{xy} were evaluated on the adhesive midline, as best representing the force/area transmitted by the adhesive.

The finite element modeling of a metal-adherend joint shows that it qualitatively matches the BEF peel stress except for a peak-truncating end effect. Over most of the joint, BEF and FEA peel results show a similar pattern with slight differences in local extrema and zero crossings. But within a region related to adhesive thickness, and depending on the adhesive Poisson ratio, the FEA peel stress suddenly reverses slope and drops well below the BEF peel stress. Thus where BEF analysis is applicable, the BEF peak is always greater than the actual FEA peak, which occurs away from

the end. We investigated the position of the actual (FEA) stress peak, and approximated the peak magnitude by truncating the BEF solution at that position.

As expected, this joint-end stress drop is primarily associated with adhesive Poisson ratio. Virtually no end effect is observed for $\nu_a = 0$, but the deviation grows for increasing ν_a, and becomes especially great above $\nu_a = 0.3$. Therefore, we sought an end-effect correction, in order that a reasonable BEF stress prediction over most of the bond could be complemented by an accurate peak value near the end. This was achieved empirically in two steps: finding a correlation for distance of the actual peel-stress peak from the joint end; then multiplying this distance times the BEF peel-stress slope at the joint end, to estimate the peak stress reduction. To carry out these steps we used the linear approximation to the BEF solution near the joint end. For a long joint, placing a new x' origin at the end of the adhesive (so $x' < 0$ represents the adhesive, see Fig. 4), we may approximate the peel-stress by the semi-infinite solution involving rightward-growing exponentials: $\frac{F(t+t_a)}{2\lambda_p^2} e^{\frac{x'}{\lambda_p}} \left[\cos(\frac{x'}{\lambda_p}) + \sin(\frac{x'}{\lambda_p})\right]$. When $x' = 0$ this reproduces the peak value σ_P given earlier. (Our occasional incorporation of t_a in the edge-bending moment was acknowledged above.) Differentiating this once and evaluating at $x' = 0$ gives the joint-edge slope $2\sigma_P/\lambda_P$.

In Fig. 5, we compare BEF and FEA peel stress distributions for a long metal-epoxy joint. Approaching the end, the sharp peak and stress drop of the blue (FEA) curve are evident. The FEA peel stress peak distance from the joint end is named $|x'_p|$. The BEF joint-end peak stress is named σ_P, and the BEF joint end peel stress slope (i.e. $2\sigma_P/\lambda_p$) is shown. To estimate the FEA peak magnitude, we moved leftward down the linear approximation for BEF by the distance $|x'_p|$. This gives the corrected peak peel stress $(\sigma_P)_{CO}$. Although this computed peak seems always to lie above the actual, even such a simple correction substantially increases the range of validity of the BEF peak stress estimation.

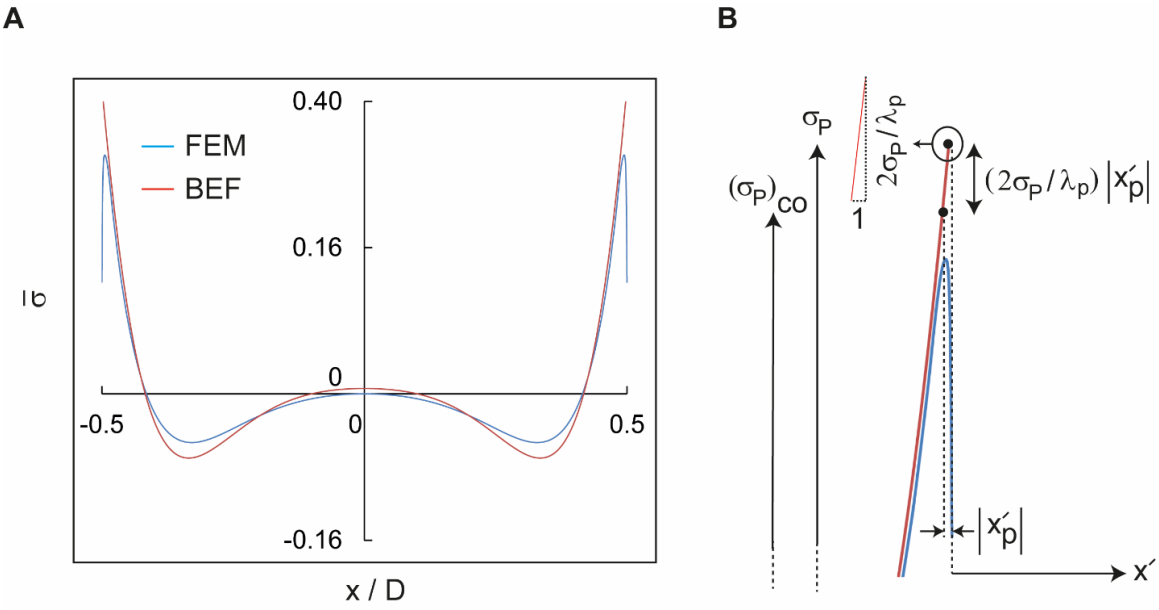

Fig.5 A) Comparison between FEA and BEF peel stress distribution for a long metal-epoxy joint. B) Poisson-driven joint end FEA peel stress drop, FEA peel stress peak distance from the joint end, $|x_P'|$, BEF joint-end peel stress slope, original and corrected BEF peak stresses are shown.

We used FEA to empirically determine peel stress peak location x'_p (a negative number) for various Poisson ratio in the realistic range 0.3 to 0.5 and sixteen different combinations of thickness and modulus ratios: $t/t_a = 2.5, 5, 10, 20$ and $\overline{E}/\overline{E}_a = 10, 100, 250, 1000$. Fig. 6A below shows $|x'_p|/t_a$, the normalized distance of peel stress peak distance from the joint end, as a function of adhesive Poisson ratio. (For clarity only four of the sixteen available curves are shown.) As shown in Fig. 6B, by normalizing $|x'_p|$ with $(t^2 t_a^2 \overline{E}/\overline{E}_a)^{1/4}$, or equivalently with $\lambda_p \left(\frac{6t_a}{t}\right)^{1/4}$, all the curves substantially collapse onto a single master curve. We therefore write $|x'_p| = f(\nu_a)\lambda_p \left(\frac{6t_a}{t}\right)^{1/4}$. A polynomial function representing $f(\nu_a)$ for $0.3 < \nu_a < 0.5$ is:

$$f(\nu_a) = 68.031{\nu_a}^5 - 72.968{\nu_a}^4 + 29.45{\nu_a}^3 - 5.344{\nu_a}^2 + 0.508\nu_a \qquad (16)$$

(Though we did not investigate it, we expect linear behavior through the origin for ν_a below 0.3.) Then the corrected peel stress peak $(\sigma_P)_{co}$ is:

$$(\sigma_P)_{co} = \sigma_P\left(1 - \frac{2|x_P|}{\lambda_p}\right) = \frac{F(t+t_a)}{2\lambda_p^2}\left(1 - 2\,f(\nu_a)\sqrt[4]{\frac{6t_a}{t}}\right), \qquad (17)$$

(Here we again used the $(t + t_a)/2$ moment arm, a major aspect of thick-adhesive analysis.) For this rough approach to make sense, the quantity subtracted from 1 must be ≤ 0.3 or so. To assure this as ν_a approaches 0.5, t_a must be less than $t/8$; this requirement is relaxed for lower values of Poisson ratio.

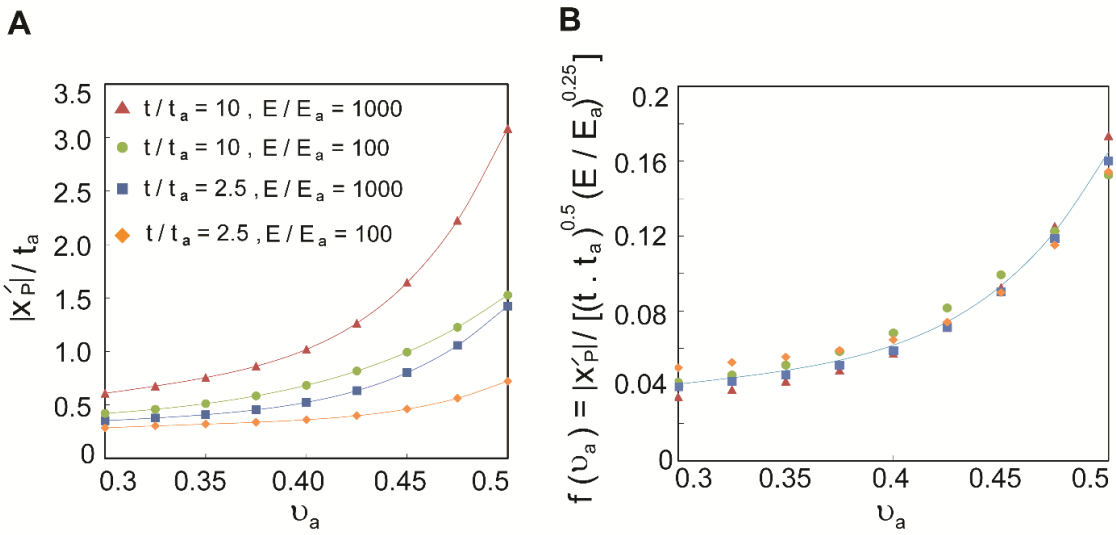

Fig. 6 A) Position $|x'_P|$ of the peel stress peak (relative to the joint end) as determined by FEA. B) The results are reasonably fitted by a polynomial in ν_a.

With this simple correction added to the BEF peak peel-stress result, we turn to its range of validity. While there are many possible ways to evaluate accuracy, we focused on 'peak peel stress' since that is the aspect most related to failure. We looked for the '110%' boundary in parameter space, namely the modulus and thickness boundary outside of which even the corrected BEF peak peel stress is 110% or more of the FEA peak stress (in our explorations it was never less). When this boundary was plotted on axes with $\log_{10}(t/t_a)$ as the abscissa, and $\log_{10}(\overline{E}/\overline{E}_a)$ as the ordinate (Fig. 7) it turned out to be a line of slope 1 for each value of ν_a, above which the accuracy is acceptable. Each line could be defined as $\overline{E}t/\overline{E}_a t_a =$ function of (ν_a), which is a ratio of the axial stiffnesses (of any chosen length) that we term R_a.

$$R_a = \bar{E}t/\bar{E}_a t_a \qquad (18)$$

This means that the adhesive layer must have sufficiently low axial stiffness, for example below 0.001 times the axial stiffness of the adherend, which particularly means that it cannot be too thick. For typical adhesive Poisson ratios, our applicability relation is thus written $R_a > 885$ ($\nu_a = 0.35$), and $R_a > 2500$ ($\nu_a = 0.4$). For example, with steel adherends 3 mm thick, to achieve accurate predictions a soft urethane adhesive of modulus 0.3 GPa might be tolerable in a thickness up to 1mm, whereas a hard epoxy adhesive of modulus 5.5 GPa might have to be thinner than 0.05 mm.

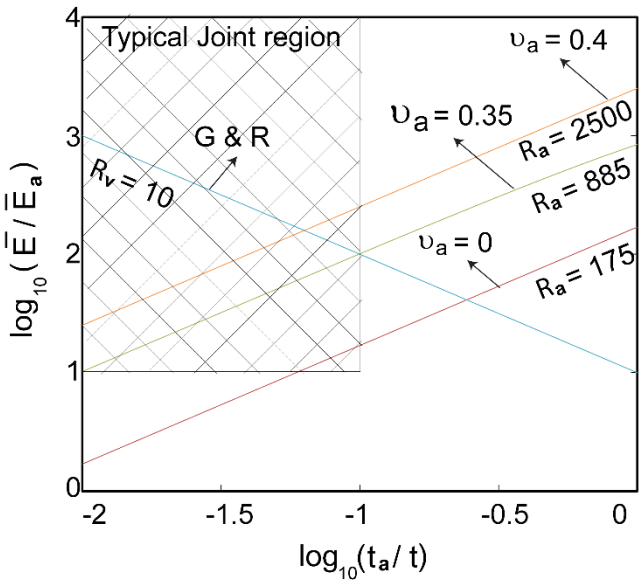

Fig. 7. Region of applicability of modified Elastic Foundation formula for long-joint peak peel stress: For each upward sloping line (dependent on adhesive Poisson Ratio), accurate predictions are expected in the direction of the arrow. For comparison, the Goland & Reissner proposed region of validity for elastic foundation analysis is shown by an arrow on the downward sloping blue line. The right half of the plot involves increasingly thick adhesive.

In 1944, Goland and Reissner proposed a criterion for applicability of BEF calculations that can be written in terms of the already-defined ratio of vertical stiffness's: $R_v = (\bar{E}/t)/(\bar{E}_a/t_a)$. They expected good BEF results for $R_v > 10$ – in other words, the adhesive layer relatively softer

than the adherend layer in the vertical direction, which implies a lower limit on t_a. This criterion is still widely quoted. In Fig. 7 the Goland and Reissner applicability criterion $R_v > 10$ is a line with slope -1, above which BEF is supposed to be accurate. Obviously the Goland and Reissner criterion is perpendicular to the 110% accuracy boundaries we found. At least in the region of typical joints (shown shaded in Fig. 7), we feel the Goland and Reissner criterion tends to be too conservative. And this conclusion is not entirely based on the empirical correction: even when no correction is applied (i.e., when Poisson ratio is zero), we find the applicability region is describable as $R_a > 175$, perpendicular to the Goland and Reissner proposed boundary and far below it.

In summary, two things were shown in this chapter. The first is that for adhesive Poisson ratios higher than 0.3 and insufficiently thin adhesive layers, the ordinary BEF peak-stress prediction for typical joints becomes more than 10% too great due to adhesive end effects, making the BEF analysis less useful. We therefore developed an empirical peak-stress correction appropriate for a wide range of joint properties and adhesive Poisson ratios. The second is that BEF peak-stress accuracy (even in the zero-Poisson case where little end-effect is observed) seems not to be meaningfully described by the Goland and Reissner applicability criterion which is defined in terms of vertical (through-thickness) stiffnesses of adherend and adhesive. A more useful criterion may be written in terms of axial stiffnesses. The way in which both criteria agree, at least in the shaded part of Fig. 7, is that increasing E_a alone should eventually render results inapplicable.

To the authors' knowledge, the Goland and Reissner proposed bound on BEF applicability have never been quantitatively confirmed. (In fact, earlier photo-elasticity experiments suggested that they are conservative.) In the range of ordinary metal-epoxy joints their recommendation seems at least one order of magnitude too strict. We have not yet uncovered cases for which the vertical stiffness ratio affects the peak stress accuracy, but that is partly because we have focused only on standard materials. (And it does seem that too low of an R_v value distorts the stress distribution in a way we didn't care about.)

Chapter 4

SIMPLIFIED EXPRESSIONS FOR JOINT-EDGE MOMENT WITH ROTATION

4. Simplified Expressions for Joint-edge Moment with Rotation

This final part of the thesis concerns the 'outer' problem: using adherend bending compliance and type of remote boundary support to estimate the force and moment applied to the joint edge. This is a geometrically nonlinear problem, in which rotation of the joint brings the joint-edge centroid closer to the load line of action, hence reducing the joint-edge bending moment. Goland and Reissner treated the outer problem for semi-infinite adherends with remote pin supports, resulting in a rather messy formula that does not reveal the moment reduction caused by finite adherends or fixed-slope supports. Zhao et al provided a simplified formula assuming a rigid overlap region with infinite pin jointed adherends. We also follow that rigid-overlap approach, in order to determine the effects of finite adherend length and pinned vs. fixed-slope supports.

It is not uncommon for an elementary lap joint illustration to display two oppositely directed adherend tensile forces with offset (i.e., out of equilibrium) lines of action. To achieve moment balance, the true joint-edge loading must include transverse forces and/or centroidal moments consistent with the boundary conditions. These extra joint-edge load components make a significant difference to the peak peel stress, which is caused primarily by the joint-edge centroidal bending moment.

For the sake of simplicity, we restrict consideration to a single lap joint loaded with 180^{o} rotational symmetry about the joint center O, see Fig. 8A. The load resultants applied to each adherend at the edge of the bonded region can be considered the sum of an axial force F at the adherend centroid, a shear force Q, and a moment M about the centroid. However, these can't be chosen arbitrarily: the assumption of 180^{o} rotational symmetry implies that the net force transmitted across the adhesive centerline passes through the adhesive midpoint (Fig. 8B). Therefore, the edge resultants must be consistent with such a force line of action.

Obviously if the transmitted force passes close to the adherend centroid at the joint edge, the joint edge bending moment magnitude will be small. The actual direction of that force (angle ψ

relative to the joint plane) depends on: the remote boundary conditions (pinned, fixed, or with springs relating displacements & rotation to adherend-end force & moment); adherend elastic properties (as might be caused by steps or taper); and the relative-motion direction of the loading grips. For low loads and fixed-slope supports, force direction at O can be determined by solving a beam problem with no transverse displacement of O. For large loads, the force direction relative to the joint plane also depends on the load-induced rotation of the overlap region, as explored below.

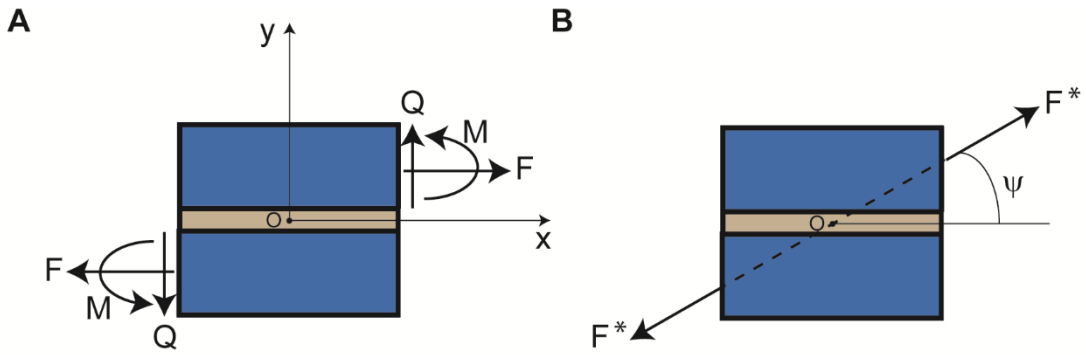

Fig. 8 A) general loading case consistent with 180^o rotational symmetry must reduce to B) a force transmitted through O.

Since the adherend bending moment at the edge of a long joint has an outsize effect on peak adhesive stress, we take the canonical loading as that which gives the largest joint-edge bending moment anticipated from standard dimensions and loading. That occurs when the adhesive-force direction is parallel to the adhesive midplane ($\psi = 0$), therefore with a moment arm relative to the adherend centroid of $a = t/2$ (or $(t + t_a)/2$ as a partial incorporation of thick-bond mechanics). We represent this load case schematically by short adherends supported at moment-free loading pins in the joint midplane (see Fig.1). Greater joint-edge moment arms seem unlikely.

The following two sub-sections explore the joint-edge moment as a function of adherend free length L, joint length D, adherend bending stiffness $\overline{E}I$, load T, and boundary conditions. Adhesive properties and thickness are disregarded. The first subsection is for a joint simply-supported at the adherend-end centroids, while the second is for fixed slope at the adherend ends. In each case, the low-load behavior, without significant rotation, is exhibited when $TL^2 \ll \overline{E}I$. (The symbol $\overline{E}$ refers

to adherend plane strain modulus, but plane stress could also be accommodated if appropriate.) Since a beam loaded with tension exhibits a characteristic length $\lambda_{bt} = \sqrt{\overline{E}I/T}$ (see Appendix 2), this expression could also be written $L \ll \lambda_{bt}$. This is the situation for short, stiff adherends weakly joined. In such cases the adhesive-force direction is found by ordinary beam analysis including the adherend end conditions.

In contrast, high-load behavior is exhibited when $TL^2 \gg \overline{E}I$ or equivalently $L \gg \lambda_{bt}$, that is, for long, slender, highly loaded adherends. Here, the force deviation is significantly affected by the load magnitude, with minimal dependence on the remote boundary conditions (pinned, fixed, etc.).

4.1) Beam-Column Result for Simply Supported Adherends

We analyze load-induced joint rotation by treating the overlap region as a rigid block of length D and width, between adherend centroids, of $t + t_a = 2a$. (This rigid-bond model differs from Goland and Reissner's assumption of nonzero bending flexibility in the overlap region.) Deformation of the non-overlapped adherend length L is analyzed with a beam-column technique adapted from Timoshenko. For our analysis, we use a rectangle to represent the rigid geometry of approximately $1/8$ of the entire overlap region. (This rectangle extends from the adhesive centerline to one adherend centerline – approximately one quarter of the overall height if the adhesive is considered thin -- over the right half of the overlap.) As seen in Fig. 9B, one corner is at adhesive centerpoint O, taken to be pinned in place for the symmetric loading where the grips each translate away from the bond. The diagonally opposite corner is point A, the point where the adherend centroid connects to the overlap region. The illustrated block is a rigid rectangle with vertical side $a = (t + t_a)/2$ reflecting the distance between the adherend centroid and the adhesive midline; and width $D/2$, since only the right half is considered.

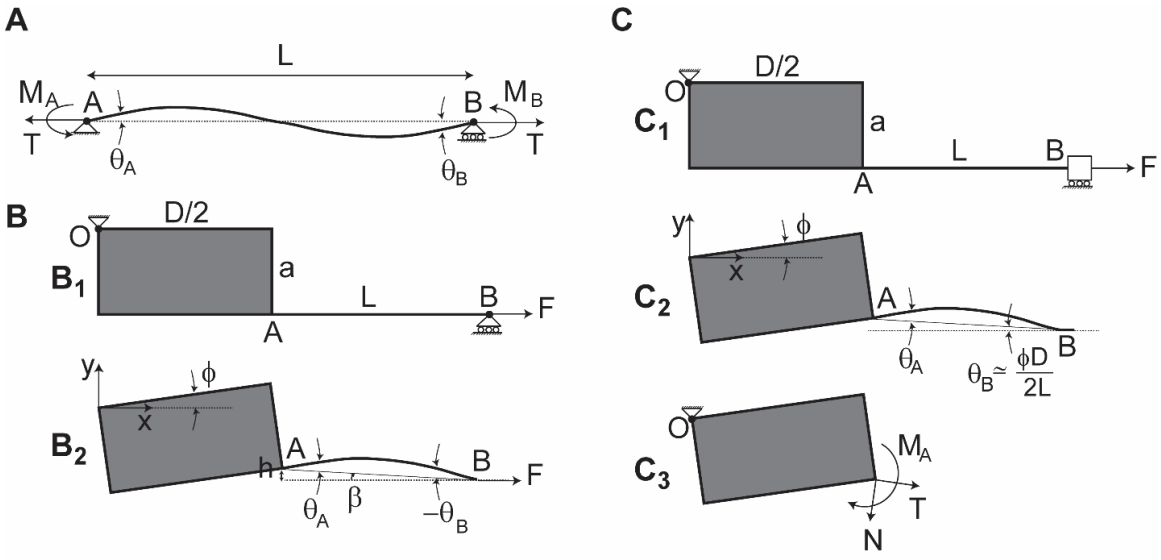

Fig. 9 A) Timoshenko beam-column under tension B) schematics of half-specimen with pinned ends, where adhesive midpoint O is fixed in space by symmetry arguments, and adherend end B translates horizontally with zero moment. a is half the centroid separation of the two adherends, and $D/2$ is half the overlap length C) schematics of half-specimen with fixed-slope ends, where adhesive midpoint O is fixed in space by symmetry arguments, and adherend end B translates horizontally with zero slope.

For these analyses we rederived the Beam-Column Equations for tensile axial load – see Appendix 2. Consider a beam of length L on simple supports at A (fixed) and B (axially translatable), subjected to tensile force T stretching the ends apart, and loaded with end moments (M_A, M_B), resulting in end slopes (θ_A, θ_B), both defined counterclockwise positive – see Fig. 9A. The end-support transverse reaction forces are not explicitly shown, but can be calculated from rotational equilibrium as $(M_A + M_B)/L$. In terms of dimensionless beam length $q = L/\lambda_{bt} = \sqrt{TL^2/\overline{EI}}$, we obtain simple, symmetric relations between end-slopes θ_A and θ_B, and moments M_A, M_B:

$$TL\theta_A = M_A H(q) - M_B K(q) \tag{19}$$

$$TL\theta_B = M_B H(q) - M_A K(q) \tag{20}$$

In these expressions:

- $H(q) = q/\tanh(q) - 1$ is positive, approximating $q^2/3$ for small q and $q - 1$ for $q > 2$. (A reasonable global approximation for $q > 0$ is $H(q) \sim q + 1.013\, e^{-1.17\, q} - 1$.)
- $K(q) = 1 - q/\sinh(q)$ is also positive, approximating $q^2/6$ for small q and 1 for $q > 4$.
- The beam-end transverse forces do not explicitly appear.

In applying these equations to one adherend joined to one eighth of the rigid bonded region, O is the fixed center of the joint, A is the beam-end centroid abutting the joint edge and B is the remote pinned beam-end centroid. In the unloaded condition, these three points are not in line. As tension increases, OA rotates by angle ϕ toward alignment with AB. At any level of tension T, we formulate the following relations:

1. The beam-column formulas. Here we use only the first formula, Eq. (19), relating M_A directly to θ_A. (The simple support condition defining $M_B = 0$ means the second equation, Eq. (20), is not needed for determining M_B.) T appears both explicitly and through its contribution to q.
2. A kinematic relation, connecting θ_A to ϕ.
3. A statical relation connecting M_A to ϕ through T and its line of action.

In principle these three relations governing M_A, θ_A, and ϕ will define M_A as a function of T.

Following are the specific equations for the pinned case ($M_B = 0$). The first beam-column formula:

$$TL\theta_A = M_A H(q) \tag{21}$$

where dimensionless load variable $q = L/\lambda_{bt} = \sqrt{TL^2/\overline{E}I}$, and $H(q)$ can be approximated as noted above. The kinematic relation:

$$\theta_A = \phi + \tan^{-1}\left(\frac{a(1-\cos\phi) + \frac{D}{2}\sin\phi}{L - a\sin\phi + \frac{D}{2}(1-\cos\phi)}\right) \tag{22}$$

For moderate values of ϕ and $a \ll L + D/2$, this expression is quite accurately approximated as $\theta_A = \phi(1 + D/2L)$. Lastly we need a third equation involving M_A, or rather the deformed-configuration moment arm at A of the force T. This is provided by the coordinate-geometry equation for the distance between point A and the OB line (since both these joints are pinned, the OB system is a two-force member):

$$\frac{M_A}{T} = \frac{aL\cos\phi - \left(a^2 + \frac{D}{2}\left(L + \frac{D}{2}\right)\right)\sin\phi}{\sqrt{a^2 + (L + \frac{D}{2})^2}} \tag{23}$$

For the moderate values of ϕ and a mentioned above, this is approximated well by:

$$\frac{M_A}{T} = \frac{aL - \phi\frac{D}{2}\left(L + \frac{D}{2}\right)}{L + \frac{D}{2}} \tag{24}$$

Eqs. (22) and (23) can be used to eliminate θ_A and M_A from Eq. (21), leaving a nonlinear equation for ϕ alone, at any value of T. Once ϕ is found by numerical iteration, M_A is known.

For plotting, we define y as Ta/M_A, or in other words (canonical moment arm a) divided by (actual loaded moment arm):

$$y = \frac{Ta}{M_A} \tag{25}$$

(Note that $y = 1/k$, where k is the edge moment factor of Goland and Reissner – this definition simplifies the mathematics.) We plot y as a function of a load variable x where

$$x = D/\lambda_{bt} = Dq/L = \sqrt{TD^2/\overline{E}I} \tag{26}$$

Note that the low-load value of y (when $\phi = 0$) is not 1 because the line between support pins passes closer than distance a to the joint-edge adherend centroid.

Fig. 10A illustrates the results, where y is plotted as a function of x with parameter L/D. To determine the edge moment in this pinned geometry, take the given tension T, multiply it by the

canonical moment arm a, and divide this moment by the plotted y value at the appropriate x (the plotted value is always ≥ 1).

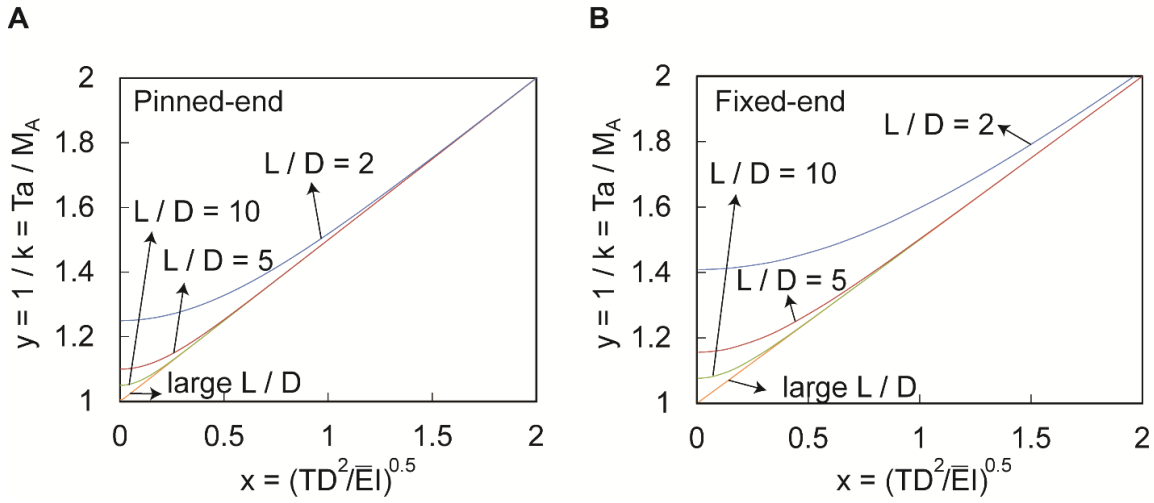

Fig. 10 A) Plot for determining edge moment of pinned-end assemblies, as a function of tensile load T. Curves are a function of L/D, approaching the straight asymptote as L/D approaches infinity. Near zero load, the moment arm is determined by the undeformed force line of action between the loading pins. B) Similar plot for determining edge moment of fixed end-slope assemblies, as a function of tensile load T. Curves are a function of L/D, where the uppermost curve has $L/D = 2$, the lowermost has $L/D = 10$, and the orange curve is for $L/D \to \infty$. At low load, the effect of a fixed-slope end on reducing moment can be deduced by a linear beam calculation.

In fact, what is actually plotted is the following expression, derived by combining the given approximations to the foregoing relations, and matching the unapproximated results with an error below about 1%.

$$y = 1 + x/2 + \frac{D}{L}(0.506)e^{-1.17x\frac{L}{D}} \qquad (27)$$

Note that as L/D approaches infinity, the relation becomes a straight line $y = 1 + x/2$. Each curve could therefore be approximated roughly as a horizontal line at low loads, switching to the asymptote at sufficient load: First, $y = 1 + 0.506\ D/L$ (in other words, moment arm $= a/(1 + 0.506D/L)$), at higher loads switching to $y = 1 + x/2$ -- in other words, to moment arm $= a/(1 +$

$0.5\sqrt{TD^2/\overline{E}I}$). The switch occurs when $x \geq 1.012D/L$, a load condition which can be expressed alternatively as $TL^2/\overline{E}I \geq 1.026$. (The limit of L/D approaching zero is somewhat problematic, because approximate joint rigidity is then no longer a good assumption.)

We may compare this result to the treatment by Goland and Reissner. They also investigated the pinned case, in the end taking $L/D \rightarrow \infty$. The main modeling difference is that they assigned bending compliance ($1/8$ that of the adherend) to the double-thickness bond region. They apparently assumed a Poisson ratio of 0.33. Expressing their parameters in terms of ours, their abscissa is $x/\sqrt{48(1-\nu^2)}$ or $x/6.54$. Their moment plot could be recast as $y = 1 + \sqrt{8}\tanh(x/2\sqrt{8})$ where ours, for infinite L/D, is $y = 1 + x/2$. The two expressions are identical for small x, and within 5% of each other as long as $x < 3$ (i.e., as long as their abscissa is below 0.45). This condition should almost always be met for elastically loaded adherends: the mean axial stress should be well under 40% of the yield strength (because of the unavoidable addition of large bending stresses). As an example for a strong steel of yield strength 1400 MPa, the maximum allowed axial stress would be 560 MPa, and their abscissa would exceed 0.45 only when $D > 36t$.

4.2) Beam-Column Result for Fixed-Slope Ends

We turn next to the case of joint rotation when adherend end-slopes are fixed. From Fig. 9C it is clear that both θ_A and θ_B, the end angles relative to AB required by beam-column analysis, are determined explicitly by ϕ. So we will use both beam-column formulas, and also expressions for θ_A and θ_B in terms of ϕ. This leads to a relation between ϕ and M_A. But ϕ is not known, it must be determined from T. Therefore, we also make use of a statics relation, stating that the forces applied to the block at point A (beam tension T along the AB line, beam transverse force N deduced from $\theta_A + \theta_B$, and beam moment M_A) must be in moment equilibrium about point O. This allows us to determine ϕ from T.

The curves developed by numerical solution of this equation are plotted in Fig. 10B. The definition of y is guided by the approximated mathematics – it is the canonical loading moment

arm, a, divided by the actual moment arm developed by tension T. The definition of x is as before, $x = D/\lambda_{bt} = \sqrt{TD^2/\overline{E}I}$. An excellent numerical fit for the L/D range shown here is given by:

$$\frac{Ta}{M_A} = 1/k = 1 + \frac{x}{2} + \frac{D}{L}\left(\frac{1+\frac{D}{L}}{\frac{4}{3}+\frac{D}{L}}\right)e^{\left(0.65-\frac{L}{D}\right)x} \tag{28}$$

It can be seen that for large x (large load), the exponential term vanishes and the relation is just a universal straight line. Whereas, for small load, short and/or stiff adherends confer protection (k is reduced).

As for the pinned case, we may further approximate the curves as two straight lines. For low loads, $\text{moment arm} = a/[1 + (D/L)(1 + D/L)/(4/3 + D/L)]$, independent of load. But when $x > 2(D/L)(1 + D/L)/(4/3 + D/L)$, or rather when $\sqrt{TL^2/\overline{E}I} > 2(1 + D/L)/(4/3 + D/L)$, then $\text{moment arm} = a/(1 + 0.5\sqrt{TD^2/\overline{E}I})$.

Summarizing: for lightly loaded joints connecting short stiff adherends, the edge moment may be approximated by classical infinitesimal-slope beam analysis involving the adherend length and boundary conditions. But for stronger joints connecting long, flexible adherends, the edge moment is reduced by joint rotation (thus requiring beam-column analysis), and at high load the moment arm becomes a function of $\sqrt{TD^2/\overline{E}I}$, where D is joint length, $\overline{E}I$ refers to the adherends, and T is the tensile load. In this situation, adherend length L becomes unimportant. The parameter defining loading regime is $\sqrt{TL^2/\overline{E}I}$.

We compared the above results to those of Zhao et al who provide exact beam-with-tension formulas for a rigid overlap and pinned-end adherends of distinct thicknesses and lengths. To simplify they take the long-adherend limit and then consider identical adherends. Their result may be written $1/k = 1 + x/2$, where ours adds moment-reducing terms based on D/L (i.e., bond length over adherend free length): see Eq. (27) for the pinned case and Eq. (28) for the fixed-end

case. These additions form the departures from a straight line (in extreme cases reaching 40%) in Fig. 10.

Another relevant paper is the work by Guo S et al They specifically addressed two factors that we ignored: the possibility of compressive loading, and misaligned (i.e., spacer-less) rigid grips that create locked-in stresses. (They also, like Goland & Reissner, included the bending of a lumped overlap region, but their results in tension validate our assumption that rigidity would serve as well.) The main differences seem to lie in the choice of variables and normalization. Guo et al present results with two different normalizations. With reference to our variables, they first give k or $1/y$ as a function of $(x/2)^2$, and then κ or $x^2/(8y)$ as a function of $(x/2)^2$. We feel that our approach with straight-line asymptotes and a reduction to just two graphs might be simpler to use. In addition, our results are encapsulated in simple empirical formulas.

Chapter 5
CONCLUSIONS

5. Conclusions

Beam on elastic foundation models for adhesive stress provide insight into the mechanics of single lap joints. The simple equations for peak stress are especially valuable. Of course the computed stresses are approximately the 'midline' through-thickness values, not the more complex distributions at the adhesive corners.

The first goal of this thesis was to establish that 'long' joints (in comparison to the characteristic distance of the elastic foundation shear stress equation) have the lowest adhesive failure stress, whether 'equivalent' or Principal. This means that designers could simply use an overlap greater than a minimum value based on joint parameters, so they can benefit from the simplest formulas and lowest values for peak stress. Our stress investigations were limited to such 'long' joints.

The peel stress formula was compared to the 'actual' peel stress found by plane strain FEA. The results were in reasonable agreement except for an end-effect that truncates the peak BEF value when Poisson's ratio is nonzero. That truncation was estimated empirically and crudely corrected. Then the applicability of the corrected peak-stress formula was compared to FEA. The match was acceptable except when the adhesive-layer axial stiffness is too high in comparison to adherend axial stiffness. This limit of applicability is quite different from Goland and Reissner's limit based on adhesive through-thickness stiffness being large in comparison to adherend through-thickness stiffness. For our definition of accuracy, within the realm of metal-epoxy joints, the Goland and Reissner criterion was at a minimum too conservative by a factor of 10.

Lastly the thesis addressed the bending moment experienced by the joint edge, since this is the main cause of peel stress. The Goland and Reissner formula is complex and not

very general. Using beam-column formulas with a rigid overlap region has resulted in relatively simple formulas for arbitrary adherend length and tension magnitude, and both pinned and fixed ends.

The results and analytical insights provided here will make it easier for engineers to estimate joint strength and optimize designs.

Chapter 6
APPENDIX

6. Appendix

This chapter has two sub-sections supplementing the thesis material.

6.1) Appendix 1: an equivalent stress for pressure-sensitive yield

Polymeric adhesives are recognized as exhibiting pressure-sensitive yielding. The simplest consequence is a difference between axial tensile yield strength and axial compressive yield strength. (See Hassanipour and Öchsner's work, their example adhesive material is stronger in compression than tension.)

In that reference, pressure-sensitivity is effected by a minimal isotropic alteration of the von Mises yield criterion, or rather the equivalent stress, by incorporating a dimensionally consistent signed contribution of the first stress invariant. (There is no discussion of an associated plastic flow rule, but this has no bearing on the problem of identifying purely elastic behavior.)

Denoting a material's compressive yield stress as $-k_c$ and tensile yield stress as k_t, where each k is a positive number, the yield criterion is given as

$$(k_c - k_t)I_1 + 3J_2 = g(\sigma_{ij}) = k_c k_t \tag{1}$$

where

$$I_1 = \sigma_{xx} + \sigma_{yy} + \sigma_{zz} \tag{2}$$

$$3J_2 = \frac{1}{2}\left[(\sigma_{xx} - \sigma_{yy})^2 + (\sigma_{yy} - \sigma_{zz})^2 + (\sigma_{zz} - \sigma_{xx})^2\right] + 3(\sigma_{xy}{}^2 + \sigma_{yz}{}^2 + \sigma_{zx}{}^2) \tag{3}$$

If we substitute either $\sigma_{zz} = k_t$ or $\sigma_{zz} = -k_c$, then $g(\sigma_{ij}) = k_c k_t$, so the yield criterion is satisfied. We may thus define an equivalent failure stress $\sigma^e = \sqrt{g(\sigma_{ij})}$ and say that yield

will occur when $\sigma^e = \sqrt{k_c k_t}$. When $k_c = k_t = Y$, then $\sigma^e = Y$, recovering ordinary von Mises yield.

Since the pressure-sensitive equivalent stress is not a homogeneous function of stress components, then unlike von Mises stress it will not be linearly proportional to load. In Hassanipour and Ochsner's work, properties for an epoxy are used, and according to Table 2 and the final line of Sec. 5, $k_c = 37.92$ MPa and $k_t = 31.60$ MPa. Then, the equivalent stress condition for pressure-sensitive yield of this adhesive is:

$$\sqrt{\begin{matrix}\frac{1}{2}\left[(\sigma_{xx}-\sigma_{yy})^2+(\sigma_{yy}-\sigma_{zz})^2+(\sigma_{zz}-\sigma_{xx})^2\right] \\ +3({\sigma_{xy}}^2+{\sigma_{yz}}^2+{\sigma_{zx}}^2)+6.32(\sigma_{xx}+\sigma_{yy}+\sigma_{zz})\end{matrix}} = 34.62 \text{ MPa} \qquad (4)$$

By deleting the term linear in σ, we recover the formula for von Mises stress.

6.2) Appendix 2: Derivation of beam-column results

The algebra of an end-loaded beam with axial tension is simplified via the symmetric beam-column formulation presented by Timoshenko, in which end-slopes relative to the mean slope are attributed to end moments, with stiffness modified by axial force. The relevant relations are derived here.

The linearized governing equation for deformation of a beam under tension T with no external transverse loads is well known: $\overline{E}I\frac{d^4w}{dx^4} = T\frac{d^2w}{dx^2}$, where $\overline{E}$ is the plane strain elastic modulus. Here, w is displacement perpendicular to the x axis, which is taken along a line from the initial position of A to the initial position of B.

We rewrite this as $\lambda_{bt}^2\frac{d^4w}{dx^4} - \frac{d^2w}{dx^2} = 0$, using a 'beam tension' characteristic length $\lambda_{bt} = \sqrt[2]{\overline{E}I/T}$.

To develop expressions that are symmetric with respect to A and B, we use the 'mean slope' coordinate axis X, which extends between the final positions of A and B, and whose origin is at the midpoint of AB. The transverse displacements W relative to this axis satisfy $W(L/2) = W(-L/2) = 0$. The equation is solved by

$$W(X) = a + bX + ce^{X/\lambda_{bt}} + de^{-X/\lambda_{bt}} \tag{5}$$

Our aim is to develop expressions that connect the end-slopes dW/dX to the end-moments. To minimize the algebra, we consider first the end moments M_A, M_B, which will allow us to determine coefficients c and d. Our convention for external applied moments is counterclockwise positive, regardless of whether the end is positive or negative. We non-dimensionalize the coordinate by λ_{bt} and employ the non-dimensional length $q = L/\lambda_{bt}$.

At ends A and B, where non-dimensional coordinates are $-q/2$ and $q/2$ respectively, we have

$$\frac{M_A}{\bar{E}I} = -\frac{d^2W}{dx^2}|_A = \frac{-1}{{\lambda_{bt}}^2}\left(ce^{-q/2} + de^{q/2}\right) \tag{6}$$

$$\frac{M_B}{\bar{E}I} = \frac{d^2W}{dx^2}|_B = \frac{1}{{\lambda_{bt}}^2}\left(ce^{q/2} + de^{-q/2}\right) \tag{7}$$

Therefore c and d may be found as

$$c = \frac{{\lambda_{bt}}^2}{\bar{E}I}\,\frac{M_A e^{-q/2} + M_B e^{q/2}}{e^q - e^{-q}} \tag{8}$$

$$d = \frac{-{\lambda_{bt}}^2}{\bar{E}I}\,\frac{M_A e^{q/2} + M_B e^{-q/2}}{e^q - e^{-q}} \tag{9}$$

(Note that the quantity $\lambda_{bt}^2/(\bar{E}I)$ may also be written as $1/T$.) To compute end-slopes we need b but not a. If we subtract the zero-displacement expression at A from that at B, then

a is eliminated and we can find $b = -\lambda_{bt}{}^2 (M_A + M_B)/(L\bar{E}I)$. With the above values of b, c, d, we can evaluate

$$\theta_A = b + \frac{c}{\lambda_{bt}} e^{-q/2} - \frac{d}{\lambda_{bt}} e^{q/2} \tag{10}$$

$$\theta_B = b + \frac{c}{\lambda_{bt}} e^{q/2} - \frac{d}{\lambda_{bt}} e^{-q/2} \tag{11}$$

Multiplying through with $L\bar{E}I/\lambda_{bt}{}^2 = LT$, we finally have

$$TL\theta_A = M_A H(q) - M_B K(q) \tag{12}$$

$$TL\theta_B = M_B H(q) - M_A K(q) \tag{13}$$

where $H(q) = q/\tanh(q) - 1$ and $K(q) = 1 - q/\sinh(q)$.

If we examine the low tension (small q) limit, we recover the slope changes due to end moments of a beam with negligible tension, e.g. $\theta_A = M_A L/(3\bar{E}I) - M_B L/(6\bar{E}I)$. On the other hand, in the high tension or long (large q) case, where string-like behavior becomes apparent, it is instructive to examine the moments under fixed angles, as q becomes large (i.e., as λ_{bt} becomes small). For example, after solving for M_A and taking the large-q limit, the behavior at A is $M_A \sim [\theta_A \sqrt{TL^2/\bar{E}I} + (\theta_B - \theta_A)\,] \,/\, [L/(\bar{E}I) - 2/\sqrt{T\bar{E}I}]$. The major part of M_A arises from the slope at A only, and grows as $\sqrt{T}$.

Qualitatively, sufficiently far (compared to λ_{bt}) from a boundary or any geometric inhomogeneity, we expect the beam, like a string, to lie along the line of the transmitted load with essentially zero bending moment. However, this straight line solution is disrupted by nonconforming boundary conditions, and most importantly by the geometry of the joint, which prevents the adherend centerlines from being collinear near the joint, within in a region of size λ_{bt}. (This is why the high-tension effect of an end slope at one end is virtually decoupled from the end slope at the other end.)

Chapter 7
REFERENCES

7. References

Ebnesajjad, S. and Landrock, A.H., Adhesives Technology Handbook. 2014: William Andrew.

Goland, M. and Reissner, E., The stresses in cemented joints. Journal of Applied Mechanics, 1944. 11(1): p. A17-A27.

Bigwood, D. and Crocombe, A., Elastic analysis and engineering design formulae for bonded joints. International Journal of Adhesion and Adhesives, 1989. 9(4): p. 229-242.

Timoshenko, S.P. and Gere, J.M., Theory of Elastic Stability, SecondEdition. 1961, McGraw-Hill.

da Silva, L.F., Öchsner, A. and Adams, R.D., Handbook of adhesion technology. 2011: Springer Science & Business Media.

Vaziri, A., Nayeb-Hashemi, H. and Hamidzadeh, H., Experimental and analytical investigations of the dynamic response of adhesively bonded single lap joints. Journal of Vibration and Acoustics, 2004. 126(1): p. 84-91.

Vaziri, A. and Nayeb-Hashemi, H., Dynamic response of tubular joints with an annular void subjected to a harmonic axial load. International Journal of Adhesion and Adhesives, 2002. 22(5): p. 367-373.

Volkersen, O., Die Nietkraftverteilung in zugbeanspruchten Nietverbindungen mit konstanten Laschenquerschnitten. Luftfahrtforschung, 1938. 15(1/2): p. 41-47.

Hart-Smith, L.J., Adhesive-bonded single-lap joints. NASA-CR-112236 1973: Langley Research Center Hampton, VA.

Luo, Q. and Tong, L., Fully-coupled nonlinear analysis of single lap adhesive joints. International Journal of Solids and Structures, 2007. 44(7): p. 2349-2370.

Adams, R. and Peppiatt, N., Stress analysis of adhesive-bonded lap joints. The Journal of Strain Analysis for Engineering Design, 1974. 9(3): p. 185-196.

Her, S.-C., Stress analysis of adhesively-bonded lap joints. Composite structures, 1999. 47(1-4): p. 673-678.

Li, G. and Lee-Sullivan, P., Finite element and experimental studies on single-lap balanced joints in tension. International Journal of Adhesion and Adhesives, 2001. 21(3): p. 211-220.

Tsai, M. and Morton, J., An evaluation of analytical and numerical solutions to the single-lap joint. International Journal of Solids and Structures, 1994. 31(18): p. 2537-2563.

Goncalves, J., De Moura, M. and De Castro, P., A three-dimensional finite element model for stress analysis of adhesive joints. International Journal of Adhesion and Adhesives, 2002. 22(5): p. 357-365.

Ashrafi, M., et al, Adhesively bonded single lap joints with non-flat interfaces. International Journal of Adhesion and Adhesives, 2012. 32: p. 46-52.

Haghpanah, B., Chiu, S. and Vaziri, A., Adhesively bonded lap joints with extreme interface geometry. International Journal of Adhesion and Adhesives, 2014. 48: p. 130-138.

Minford, J.D., Handbook of aluminum bonding technology and data. 1993: CRC Press.

Adams, R.D., Comyn, J. and Wake, W.C., Structural adhesive joints in engineering. 1997: Springer Science & Business Media.

Zhao, X., Adams, R. and da Silva, L.F., A new method for the determination of bending moments in single lap joints. International Journal of Adhesion and Adhesives, 2010. 30(2): p. 63-71.

Hassanipour, M. and Öchsner, A., Implementation of a pressure sensitive yield criterion for adhesives into a commercial finite element code. The Journal of Adhesion, 2011. 87(12): p. 1125-1147.

Guo, S., Dillard, D.A. and Plaut, R.H., Effect of boundary conditions and spacers on single-lap joints loaded in tension or compression. International Journal of Adhesion and Adhesives, 2006. 26(8): p. 629-638.